How to match an acoustical load to a thermoacoustic heat engine?

Cite as: AIP Conference Proceedings **1573**, 1445 (2014); https://doi.org/10.1063/1.4860877
Published Online: 17 February 2015

L. M. Zhang, Y. Y. Chen and E. C. Luo

How to Match an Acoustical Load to a Thermoacoustic Heat Engine?

L. M. Zhang[a, b], Y.Y.Chen[a], E. C. Luo[a]

[a]*Key Laboratory of Cryogenics, Technical Institute of Physics and Chemistry, Chinese Academy of Sciences, Beijing 100190, China*
[b]*Graduate University of the Chinese Academy of Sciences, Beijing 100049, China*

Abstract. The efficient operation of a thermoacoustic prime mover and its acoustic load depends on whether they match each other. In this paper, a numerical simulation of RC-type and RL-type acoustic loads driven by a traveling-wave thermoacoustic engine with constant heating temperature was carried out. It is found that the dependence of the output acoustic power and efficiency on the acoustic load is quite complicated and unique. There are several critical acoustic loads which can characterize the unique output performance of the acoustic heat engine. In addition, a trade-off between net acoustic power and thermal efficiency needs to be made. This work is helpful to provide guidance on how to design an efficiently loaded thermoacoustic engine.

Keywords: Traveling-wave thermoacoustic engine, RC-type load

INTRODUCTION

As a new type of heat engine, the thermoacoustic-Stirling heat engine has attracted worldwide attention for its high efficiency, simple configuration, environment-friendly working gas and good adaptability of using various heat resources [1]. Thermoacoustic engines can drive different acoustic loads to form different thermoacoustic systems, such as thermoacoustically-driven pulse tube refrigerators [2-4], and thermoacoustically driven electricity generators [5, 6]. The performance of a whole thermoacoustic system depends not only on the thermoacoustic heat engine itself but also on its driving loads. A few numerical simulations and experimental research studies on the thermoacoustically-driven RC-type acoustic load systems operating with constant heating power have been reported [7, 8], which showed that a maximum acoustic power and thermal efficiency can be obtained when the resistive impedance of an RC-type acoustic load equals its capacitive impedance. However, thermoacoustic-driven systems usually operate with constant heating temperature. One reason is that the temperature of the heat source is usually given, and the other is that the operation of a thermoacoustic heat engine is restricted by the allowable temperature of its used structure material. Thus, the heating temperature must be limited below a certain range. In this paper, a numerical simulation of RC-type and RL-type acoustic loads driven by a traveling-wave thermoacoustic engine with constant heating temperature is carried out, in order to figure out how to match an acoustic load to a thermoacoustic heat engine.

COMPUTATIONAL MODEL

According to the classical thermoacoustic theory [9], momentum, continuity and energy equations for a short channel can be written as:

$$\frac{dp_1}{dx} = -\frac{i\omega\rho_m}{A(1-f_v)}U_1 \tag{1}$$

$$\frac{dU_1}{dx} = -\frac{i\omega A}{\gamma p_m}\left(1+\frac{(\gamma-1)f_\kappa}{1+\varepsilon_s}\right)p_1 + \frac{(f_\kappa - f_v)}{(1-f_v)(1-\sigma)(1+\varepsilon_s)}\frac{1}{T_m}\frac{dT_m}{dx}U_1 \tag{2}$$

$$\frac{d\dot{H}_2}{dx} = \dot{q} \tag{3}$$

Advances in Cryogenic Engineering
AIP Conf. Proc. 1573, 1445-1452 (2014); doi: 10.1063/1.4860877

$$\dot{H}_2 = \frac{1}{2}\mathrm{Re}[p_1\tilde{U}_1(1-\frac{f_\kappa-\tilde{f}_\upsilon}{(1-f_\upsilon)(1-\sigma)(1+\varepsilon_s)})]+$$
$$\frac{\rho_m c_p |U_1|^2}{2A\omega(1-\sigma)|1-f_\upsilon|^2}\frac{dT_m}{dx}\mathrm{Im}[\tilde{f}_\upsilon+\frac{(\tilde{f}_\kappa-\tilde{f}_\upsilon)(1+\varepsilon_s f_\upsilon/f_\kappa)}{(1+\varepsilon_s)(1-\sigma)}]-(Ak+A_s k_s)\frac{dT_m}{dx} \quad (4)$$

where p_1 and U_1 are the first-order pressure amplitude and volume velocity amplitude, i is the imaginary symbol, ω is the angular frequency ($\omega = 2\pi f$, f is the operating frequency), A is the cross-sectional area of the channel, ρ_m, p_m, T_m are the mean density, pressure and temperature of the working gas, γ, c_p, k, σ are the specific heat ratio, isobaric specific heat capacity, thermal conductivity and Prandtl number of the working gas, complex function f_υ and f_κ , which depend on the specific channel geometry and the gas properties are detailed defined in Reference [9], A_s and k_s are the cross-sectional area and thermal conductivity of the channel solid, ε_s is a correction for thermal properties of the solid wall, Re and Im mean taking the real part and imaginary part, respectively, ~ means complex conjugate, | | means the magnitude of a complex number. $\dot{H}_2$ is the total power, and $\dot{q}$ is the heat added per unit length.

Figure 1 shows the schematic of the traveling-wave thermoacoustic-driven RC-type acoustic load system, which consists of a feedback tube, the main water-cooled heat exchanger (MHX), regenerator, heater, thermal buffer tube (TBT), secondary water-cooled heat exchanger (SHX) and resonator. The resonator is composed of two sections: one is the tapered section with the inner diameter from 100mm to 300mm and the length of 4.3m, and the other is a cylindrical section with the inner diameter of 300mm and the length of 1m. The main dimension of the engine is listed in Table I. More detailed dimensions are given in Reference [10]. The RC-type acoustic load consists of a needle valve and a gas reservoir.

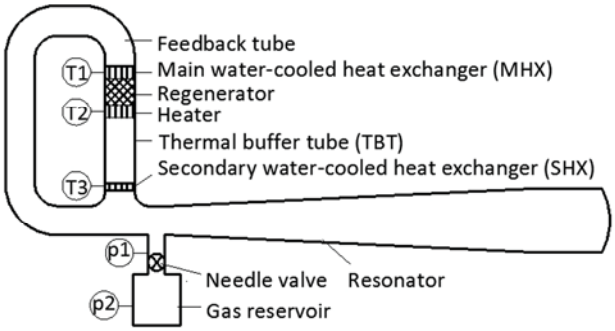

FIGURE 1. Schematic of the Traveling-wave Thermoacoustic-driven RC-type Acoustic Load System.

TABLE 1. Dimensions of the Traveling-wave Thermoacoustic-driven RC-type Acoustic Load System

Components	Diameter/mm	Length/mm
Feedback tube	100	1345
MHX	100	50
Regenerator	100	80
Heater	100	60
TBT	100	240
SHX	100	20
Resonator	100 to 300	4300+1000

The impedance of the needle valve can be simulated as a acoustic impedance R . The impedance of the reservoir can be simulated as a capacitive acoustic impedance $1/(i\omega C)$, where $C = V/(\gamma p_m)$, V is the volume of the reservoir. So, the acoustic impedance of the RC-type acoustic load is expressed as $Z = R + 1/(i\omega C)$. The oscillating

volumetric velocity amplitude at the load inlet (U_L), the phase between pressure and volume velocity at the load inlet (θ_L), and the acoustic power delivered to the RC load (W_L) can be expressed as follows:

$$U_L = \frac{p_L}{R + 1/(i\omega C)} \tag{5}$$

$$\theta_L = \arctan(-1/(\omega CR))\theta_L = \arctan(-1/(\omega CR)) \tag{6}$$

$$W_L = \frac{1}{2}|p_L||U_L|\cos(\theta_L) = \frac{1}{2}R|U_L|^2 \tag{7}$$

where, p_L is the first-order oscillating pressure amplitude at the inlet of the load. The thermal efficiency of thermoacoustic system (η_L) is defined as:

$$\eta_L = \frac{W_L}{Q_L} \tag{8}$$

where, Q_L is the heating power of the heater.

The computation is performed by using the DeltaEC6.2 software [10], which was developed by the Los Alamos National Laboratory. Based on the classical thermoacoustic theory, the DeltaEC (Design Environment for Low-Amplitude Thermoacoustic Energy Conversion) is the computation software of thermoacoustic equipment, which includes modules for heat exchangers, regenerators, ducts, acoustic compliance, and pistons, etc. The thermoacoustic system can be simplified as some modules to be simulated. The simulation is carried out under constant heating temperature (T_h) of 923K (650 $^\circ C$), a mean pressure of 3.5MPa with the working gas of helium. The environment temperature is 303K (30 $^\circ C$).

RESULTS AND DISCUSSION

RC-type Acoustic Load

Usually, the measurement for the net acoustic power output of a thermoacoustic-Stirling heat engine uses the above-mentioned RC-type load, shown in Figure 1. Here, a needle valve and an empty reservoir form the RC-type acoustic load. Due to the capacitive impedance of the reservoir, the imaginary part of the acoustic load Z is always negative. However, the imaginary part of a practical acoustic load can be positive (i.e. inductive). For instance, when the thermoacoustic-Stirling heat engine is coupled with a linear electricity generator, the imaginary part of its equivalent acoustic impedance can be positive or negative, depending on the spring stiffness and the moving mass of the linear alternator. Regardless of what the thermoacoustic-Stirling heat engine is coupled with, we can adopt a virtual positive volume reservoir to simulate the capacitive part of an RC-type acoustic load or negative volume reservoir to simulate the inductive part of an RL-type acoustic load.

In this section, the simulation was carried out for different positive-volume reservoirs: 0.5L, 0.84L, 2L, 2.67L and 7L. Figures 2 to 7 show the computed curves. It must be pointed out that there are no convergent solutions in the range of resistive impedance changing from 3.4×10^5 to 8.8×10^6 Pa·s/m^3 for a 7L reservoir. It indicates that the thermoacoustic system cannot be operated within this impedance range, which is consistent with the practical situation in our experiments. In other words, the load with the reservoir of 7L is too large for this thermoacoustic engine.

Figures 2 and 3 show the oscillating pressure amplitude at the load inlet p_L, and the heating power of the heater Q_L depending on the resistive impedance R of the RC-type acoustic load. Operating with the constant heating temperature, p_L and Q_L have the same tendency. When R is small enough, i.e. $R << 1/(\omega C)$, p_L and Q_L are almost independent of R. Under this condition, the capacitive impedance is the decisive factor for the thermoacoustic system. A larger reservoir results in smaller p_L and Q_L. When R is in the middle range, both R and $1/(\omega C)$ are equally important. It can be noted that there is a minimum value of pressure amplitude for each

curve (except for 7L reservoir) in Figure 2, and a minimum value of heating power for each curve in Figure 3. A larger reservoir volume results in a lower minimum value. When R is large enough, i.e. $R >> 1/(\omega C)$, R is dominant with the curves coincident for different reservoirs.

The dependence of the frequency on the resistive impedance is shown in Figure 4. There is a minimum value in each curve (except for 7L reservoir). Figure 5 shows the phase angel of the load θ_L with respect to the resistive impedance. The output acoustic power W_L distribution is shown in Figure 6. As seen in Figure 6, the dashed lines show that there is a maximum acoustic power value for the reservoir of 0.5L or 0.84L. Meanwhile, θ_L equals to -45°, and p_L and Q_L are minimum. That is to say that the main acoustic power generated by the regenerator is dissipated by the RC-type acoustic load when R equals to $1/(\omega C)$. In this case, the oscillating flow is weakened in the thermoacoustic system, in which less heating power is needed. It also demonstrates that the larger the reservoir is, the higher the maximum acoustic power delivered to the load is. This acoustic power output characteristic is similar to the characteristic of the thermoacoustic system operating with constant heating power in References [7], and that operating with constant pressure ratio at the RC-type acoustic load inlet reported in Reference 8. But the difference is that there are two maximum values of acoustic power output for the reservoir being larger than 0.84L. We here define the 0.84L reservoir as the first critical volume (Vcr1). The minimum values of acoustic power are obtained at the phase angle of -45°, which means that the resistive impedance value is equal to the capacitive impedance. In this condition, the acoustic field in the regenerator is unable to amplify acoustic power, and a higher heating temperature is needed. In other words, the constant heating temperature of 923K limits the acoustic power generation and leads to a small acoustic power delivered to the load, and even prevents the engine from driving the load when the reservoir is too large. In addition, when the reservoir is larger than 2.67L, the net acoustic power output curve becomes discontinuous. We define the value of 2.67L as the third critical volume (Vcr3). The second critical volume will be defined in the following paragraph).

Figure 7 presents the dependence of the thermal efficiency η_L on the resistive impedance R with different reservoirs. When the reservoir is smaller than 2L, η_L reaches its maximum value at the phase of -45°. For the 2L reservoir, there is still only one maximum value for the thermal efficiency, but there are already three extreme value points of the acoustic power delivered to the load, two maximum values and one minimum value (see Figure 6). We here define the 2L volume reservoir as the second critical volume (Vcr2). When the reservoir is larger than 2L, the curve of η_L displays two maximum values. It can be seen from Figures 6 and 7 that W_L does not follow η_L. W_L and η_L reach their maximum values at different resistive impedance values for the same reservoir. Thus, a compromise consideration is needed when the thermoacoustic-driven system is designed.

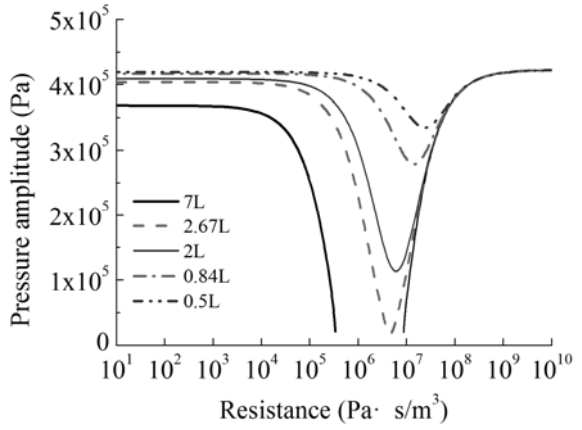

FIGURE 2. Oscillating Pressure Amplitude

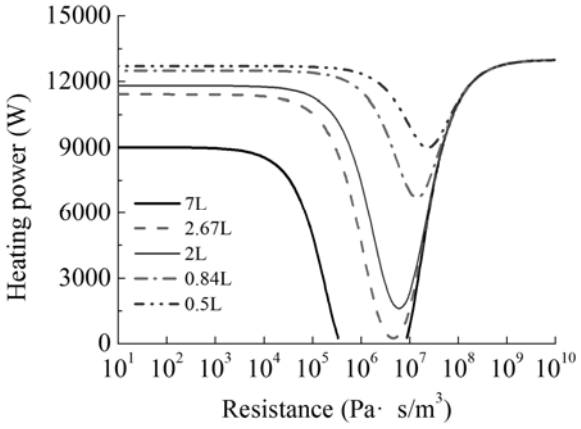

FIGURE 3. Heating Power

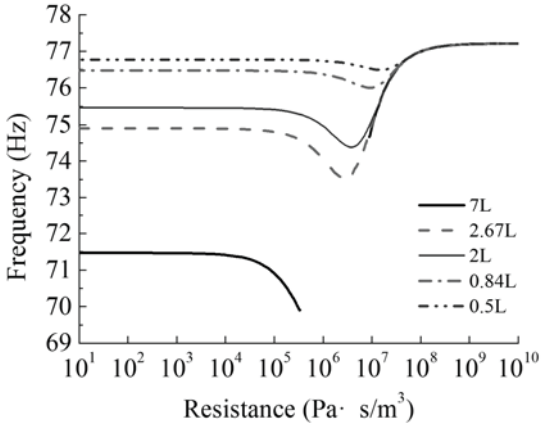

FIGURE 4. Resonant Frequency

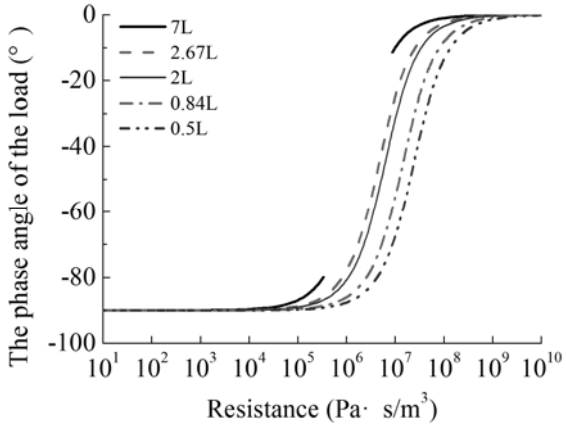

FIGURE 5. Phase Angle of the Acoustic Load

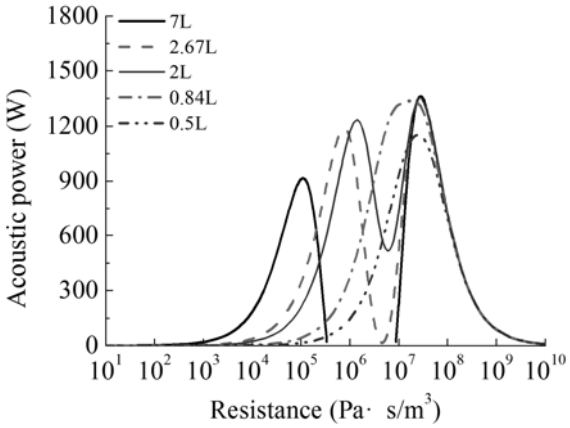

FIGURE 6. Net Acoustic Power Delivered to the Load

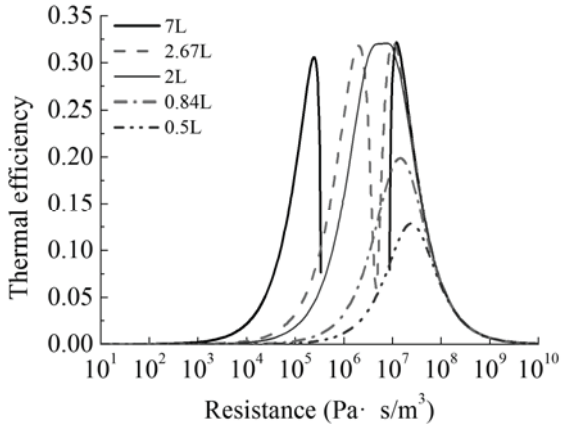

FIGURE 7. Thermal Efficiency of the System

RL-type Acoustic Load

For a linear alternator, the acoustic-electrical equations can be described approximately as [9]:

$$(R_{elec} + iX_{elec})I_1 = \frac{\tau}{A}U_1 \tag{9}$$

$$\Delta p_1 = \frac{\tau}{A}I_1 + \frac{R_{mech} + iX_{mech}}{A^2}U_1 \tag{10}$$

These two equations express Ohm's law and Newton's law, respectively. U_1 is the complex volume velocity of the piston's motion. I_1 is the complex electric current through the alternator. Δp_1 is the complex pressure difference on the front and back sides of the moving piston. τ is the transduction coefficient which is also called the "BL product". R_{elec} is electric resistance, and $X_{elec} = \omega L_{elec}$ is electric reactance, where L_{elec} is electric inductance. R_{mech} is mechanical resistance, and $X_{mech} = \omega M - K / \omega$ is mechanical reactance, where M is mass of the piston and K is spring constant. Combining Equations (9) and (10) by eliminating I_1 easily yields the acoustic impedance of the alternator as follows:

$$Z_a = -\frac{\Delta p_1}{U_1} = \frac{(\tau / A)^2}{R_{elec} + iX_{elec}} + \frac{R_{mech} + iX_{mech}}{A^2} \tag{11}$$

The positive imaginary part of the acoustic impedance may appear in thermoacoustic-driven alternators. For example, if $L_{elec} = 0$, which leads to $X_{elec} = 0$, and $K < \omega^2 M$, the imaginary part of the acoustic impedance of the alternator $\mathrm{Im}[Z_a] = (\omega M - K/\omega)/A^2$ will be positive. In order to simulate the acoustic impedance with a positive imaginary part, a negative-volume reservoir is introduced here. Figures 8 to 13 show the computed curves. As seen in Figure 12, the output acoustic power reaches the maximum when R equals to $1/(\omega C)$, and two peaks appear when the reservoir is larger than 0.82L (the first critical volume), which is similar to the case in which the imaginary part of the acoustic impedance is negative. If the volume is larger than 2L (the second critical volume), the thermal efficiency curve will display two maximum values, as seen in Fig.13. The net acoustic power output curve becomes discontinuous when the volume reservoir is larger than 2.81L (the third critical volume). The difference is that the left peak of acoustic power increases with the increase of the reservoir's volume at first and then decrease when the reservoir is larger than 13.5L. Correspondingly, when R is small enough, i.e. $R << 1/(\omega C)$, with the reservoir increasing, p_L and Q_L increase firstly and then decrease. And the larger reservoir results in higher frequency. However, compared to Figures 7 and 13, the efficiency distribution is very similar for positive and negative reservoirs.

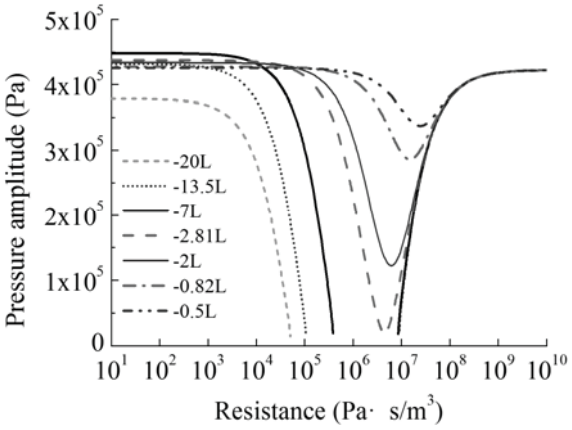

FIGURE 8. Oscillating Pressure Amplitude at the Load Inlet

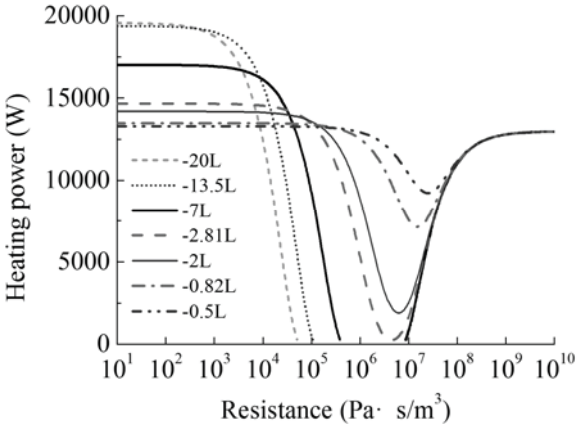

FIGURE 9. Heating Power

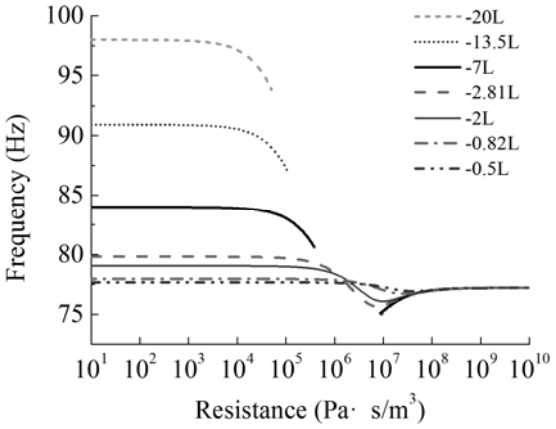

FIGURE 10. Resonant Frequency

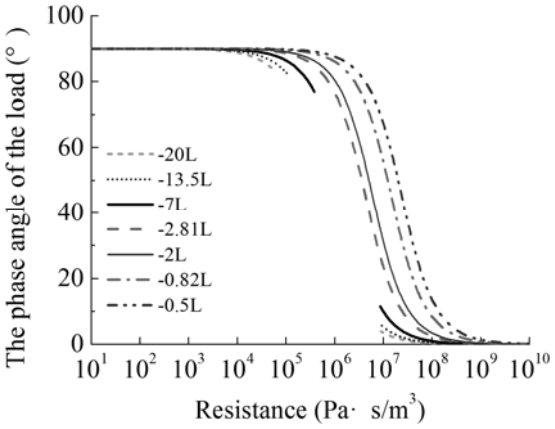

FIGURE 11. Phase Angle of the Acoustic Load

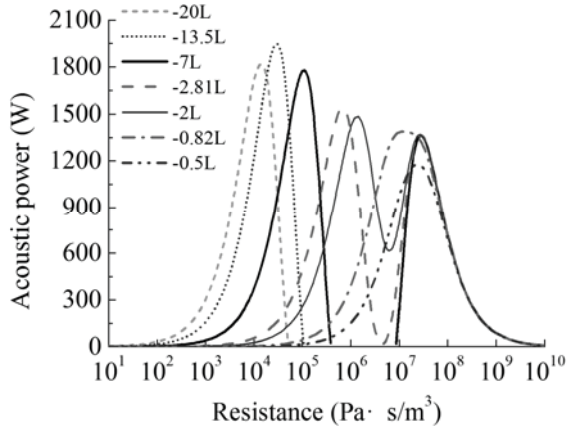

FIGURE 12. Net Acoustic Power at T_h=923K

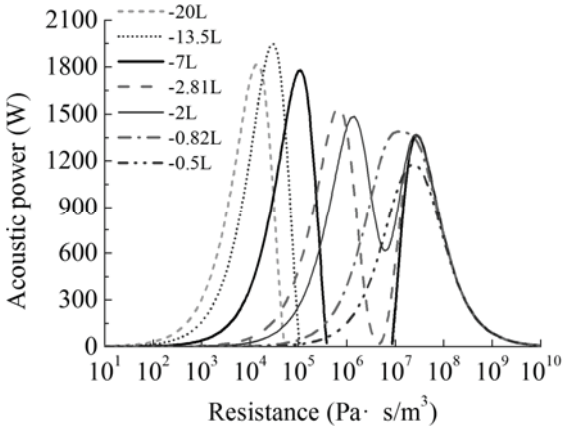

FIGURE 13. Thermal Efficiency at T_h=923K

EXPERIMENTAL COMPARISON

Some experiments were performed with helium as the working gas, a mean working pressure of 3.5MPa and constant heating temperatures. The schematic of the experimental apparatus is shown in Figure 1. Three temperature measuring points are located at MHX, heater and SHX. Temperatures are measured with NiCr-NiSi thermocouples. Two pressure transducers are fixed at the inlet of the load and the gas reservoir. The gas reservoir volume is 7L. MHX and SHX are cooled by chilled water at 303K.

Based on the measurement, R of the load and the acoustic power delivered to the load W_L are:

$$R = \frac{p_{1,1} - p_{1,2}}{U_L} = \frac{\gamma p_m |p_{1,1}|}{\omega V |p_{1,2}|} \sin\theta_{p_{1,1}-p_{1,2}} \tag{12}$$

$$W_L = \frac{1}{2}\mathrm{Re}[p_{1,1}\tilde{U}_L] = \frac{\omega V}{2\gamma p_m}\mathrm{Im}[p_{1,1}\tilde{p}_{1,2}] = \frac{\omega V}{2\gamma p_m}|p_{1,1}||p_{1,2}|\sin\theta_{p_{1,1}-p_{1,2}} \tag{13}$$

where, $p_{1,1}$ and $p_{1,2}$ are the first-order of complex pressure at the load inlet and the gas reservoir, respectively; $\theta_{p_{1,1}-p_{1,2}}$ is the phase difference between $p_{1,1}$ and $p_{1,2}$.

Figure 14 and 15 show the experimental data and corresponding computed curves. The dependence of acoustic power delivered to the load and the thermal efficiency on resistive impedance under a constant heating temperature of 923K is shown in Figure 14. In the experiment, an acoustic power of 1220.9W is obtained, with a thermal efficiency of 23.5%. The computed curves show that the efficiency of 25% corresponds to four resistive impedance points with different acoustic power delivered to the load. It implies that the match between thermoacoustic engine and the load should be considered carefully. For the same thermal efficiency, there could be four different net acoustic power outputs if the RC-load is different under the same heating temperature. In other words, there might be four possible steady operating states for the same thermal efficiency even under the same heat temperature.

Figure 15 presents the dependence of acoustic power delivered to the load on the resistive impedance with different heating temperatures of 923K, 823K, 723K and 623K, respectively. The behavior of the experimental results is consistent with the computational curves. Two maximum acoustic power values for each operating condition are presented in the computed curves. The acoustic power delivered to the load decreases with the decrease of heating temperature. In the experiment, the right branch curves for the net acoustic power output are obtained for heating temperatures of 723K and 623K, respectively. Unexpectedly, restricted by the limited adjustability of the needle valve, its effective acoustic resistance cannot be finely tuned by gradually adjusting its opening, so the left branch curve has not yet been obtained in the present experiment. Nevertheless, good agreement between the obtained experimental and computational data indicates the creditability of the simulation and analysis.

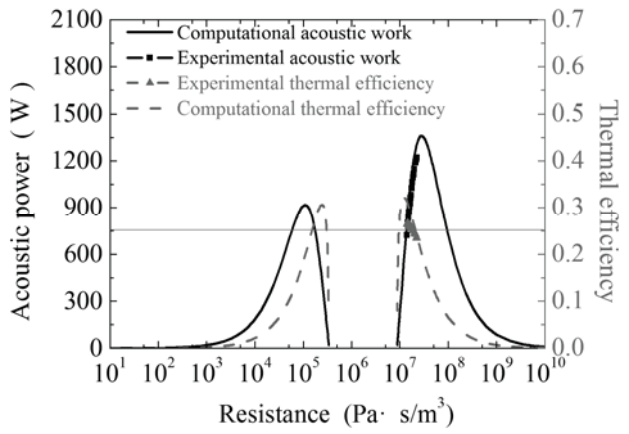

FIGURE 14. Acoustic Power and Thermal Efficiency at 923K

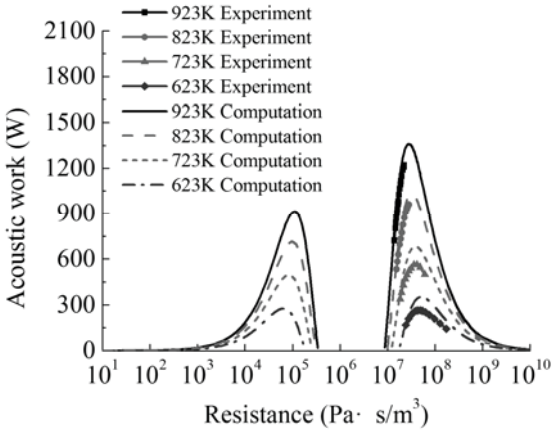

FIGURE 15. Acoustic Power under Different T_h

CONCULSIONS

The simulation of the traveling-wave thermoacoustic-driven RC-type and RL-type acoustic load system operating with constant heating temperature shows that the characteristic of the system is greatly influenced by the coupled load. The dependence of the output acoustic power and thermoacoustic conversion efficiency on the acoustic load is complicated and unique. Several maximum or minimum values can exist, depending upon the coupled acoustic loads. Furthermore, the net acoustic power and the thermal efficiency cannot reach their maximums synchronously. Therefore, a compromise for balancing acoustic power and thermal efficiency should be made.

In addition, an experimental thermoacoustic-Stirling engine was constructed to compare with the theoretical prediction, showing a reasonable agreement. In the experimental system, the maximum acoustic power of 1220.9W with a thermal efficiency of 23.5% was obtained in our experimental travelling-wave system. It is believed that the acoustic power output characteristic of the thermoacoustic system presented in this paper is very helpful for understanding and designing the thermoacoustically driven systems for some practical applications.

ACKNOWLEDGMENTS

This work was financially supported by the Basic Research Program of Chinese Sciences and Technology Ministry (Contract No.2010CB227303), the Key Project of Chinese Academy of Sciences(Contract No.KGCX2-YW-379) and the Director Project of the Technical Institute of Physics and Chemistry of CAS (Contract No. Y1A90311G1).

REFERENCES

1. Ray Radebaugh, *J.phy. Condens. Matter* **21**, 164219 (2009).
2. J.Y. Hu, E.C. Luo, W. Dai, and Y. Zhou, *Chin. Sci. Bull.* **52**, 574-576 (2007).
3. J.Y. Hu, E.C. Luo, S.F. Li, B. Yu, and W. Dai, *J. Appl. Phy.* **103**,104906 (2008).
4. S.L. Zhu, G.Y. Yu, E.C. Luo, Z.H. Wu, and X.D. Zhang, *Cryogenics* **49**, 51-54 (2009).
5. Z.H. Wu, M. Man, E.C. Luo, W. Dai, and Y. Zhou, *Chin. Sci. Bull.* **56**, 1975-1977 (2011).
6. S. Backhus, E. Tward, and M. Petach, *Appl. Phys. Lett.* **85**, 1085-1087 (2004).
7. R. Bao, G.B. Chen, K. Tang, Z.Z. Jia, and W.H. Cao, *Cryogenics* **46**, 666-671 (2006).
8. D.M. Sun, L.M. Qiu, B. Wang, Y. Xiao, and L. Zhao, *Energy Conversion and Managemnet* **49**, 1265-1270 (2008).
1. Swift GW, *Thermoacoustics: a unifying perspective for some engines and refrigerators,* Sewickley PA: Acoustical Society of America Publications Publication, 2002.
9. M. Man, "Study on the Operating Principle of Traveling-wave Thermoacoustic Electrical Generator", Ph. D thesis, Technical Institute of Physics and Chemistry, Chinese Academy of Sciences, Beijing, 2008, in Chinese.
10. B. Ward, J. Clark and G. Swift, "Design Environment for Low-Amplitude ThermoAcoustic Energy Conversion, DELTAEC Version6.2 Users Guide", 2008.